Line-Enhanced Deformable Registration of Pulmonary Computed Tomography Images Before and After Radiation Therapy With Radiation-Induced Fibrosis

Martin King, MD, PhD[1], William F. Sensakovic, PhD[2], Peter Maxim, PhD[1], Maximilian Diehn, MD, PhD[1], Billy W. Loo, MD, PhD[1], and Lei Xing, PhD[1]

Abstract

Purpose: The deformable registration of pulmonary computed tomography images before and after radiation therapy is challenging due to anatomic changes from radiation fibrosis. We hypothesize that a line-enhanced registration algorithm can reduce landmark error over the entire lung, including the irradiated regions, when compared to an intensity-based deformable registration algorithm. **Materials:** Two intensity-based B-spline deformable registration algorithms of pre-radiation therapy and post-radiation therapy images were compared. The first was a control intensity–based algorithm that utilized computed tomography images without modification. The second was a line enhancement algorithm that incorporated a Hessian-based line enhancement filter prior to deformable image registration. Registrations were evaluated based on the landmark error between user-identified landmark pairs and the overlap ratio. **Results:** Twenty-one patients with pre-radiation therapy and post-radiation therapy scans were included. The median time interval between scans was 1.2 years (range: 0.3-3.3 years). Median landmark errors for the line enhancement algorithm were significantly lower than those for the control algorithm over the entire lung (1.67 vs 1.83 mm; $P < .01$), as well as within the 0 to 5 Gy (1.40 vs 1.57; $P < .01$) and >5 Gy (2.25 vs 3.31; $P < .01$) dose intervals. The median lung mask overlap ratio for the line enhancement algorithm (96.2%) was greater than that for the control algorithm (95.8%; $P < .01$). Landmark error within the >5 Gy dose interval demonstrated a significant inverse relationship with post-radiation therapy fibrosis enhancement after line enhancement filtration (Pearson correlation coefficient = −0.48; $P = .03$). **Conclusion:** The line enhancement registration algorithm is a promising method for registering images before and after radiation therapy.

Keywords

deformable registration, line enhancement, radiation therapy, lung

Abbreviations

CT, computed tomography; EBRT, external beam radiation therapy; EQD2, equivalent dose in 2 Gy fractions; GTV, gross tumor volume; IQR, interquartile range; LUL, left upper lobe; NCC, normalized correlation coefficient; RT, radiation therapy; RUL, right upper lobe; SBRT, stereotactic body radiation therapy.

Received: August 1, 2017; Revised: October 23, 2017; Accepted: November 22, 2017.

Introduction

The accurate deformable registration of pulmonary computed tomography (CT) images before and after radiation therapy (RT) would be an important advancement in the current era of quantitative imaging. From a clinical standpoint, such a tool could dramatically enhance treatment planning for the reirradiation of pulmonary nodules. Given the potential link between

[1] Department of Radiation Oncology, Stanford University School of Medicine, Stanford, CA, USA
[2] Department of Radiology, Florida Hospital, Orlando, FL, USA

Corresponding Author:
Martin King, Brigham and Women's Hospital and Dana-Farber Cancer Institute, 75 Francis St., ASB1-L2, Boston, MA 02115, USA.
Email: martin_king@dfci.harvard.edu

radiation pneumonitis and dosimetric indices,[1-3] minimization of dose to previously irradiated regions may reduce the risk of radiation pneumonitis. Accurate mapping of pre-RT and post-RT images, especially within irradiated regions, would be essential for such a task. Furthermore, accurate deformable registration could provide improved anatomical and functional dose–response modeling regarding the late effects of RT.[4-6]

The deformable registration of pre-RT and post-RT images is a challenging task. Current registration algorithms, which are often used for registering images from a 4D-CT data set or inhalation–exhalation breath-hold images, assume a one-to-one correspondence between the 2 images being registered. This assumption would be violated with gross anatomic changes induced by radiation fibrosis and/or tumor growth. As a result, deformable registration algorithms may lead to artificial warping around irradiated tumors.[7] In order to reduce artificial warping that could be present in the longitudinal assessment of tumor nodules on CT, investigators have incorporated rigidity[8] and topology-preserving constraints[9] into deformable registration algorithms. Another group utilized a Hessian-based line enhancement algorithm for the deformable registration of images obtained before and 3 weeks after RT.[10]

The purpose of this article is to evaluate the incorporation of a Hessian-based line enhancement algorithm[11] into a deformable registration algorithm[12] for the registration of pre-RT and post-RT images obtained months to years after completion of RT. The registration of such images is challenging, due to the development of radiation-induced fibrotic changes or the growth of tumors within or outside of the radiation field. We anticipate that the Hessian-based line enhancement filter can augment linear structures including the pulmonary bronchi and vessels while suppressing large homogeneous fibrotic regions often found in post-RT images. We hypothesize that line-enhanced registrations can reduce landmark error over the entire lung and within irradiated regions when compared to an intensity-based deformable registration algorithm.

Methods

Image Database

An institutional review board–approved retrospective study of patients, who underwent 2 consecutive RT courses between January 2007 and January 2013, was conducted. Patients who had prior surgery, prior RT, or severe pulmonary pathology (eg, pleural effusion, concurrent pneumonia, and severe granulomatous disease) were excluded. All CT scans were acquired using the GE Discovery ST Multislice positron emission tomography/CT scanner (GE Healthcare, Waukesha, Wisconsin). Treatment planning scans were acquired at end-exhalation breath hold in helical mode at 120 kVp, 440 mAs, 1.25 mm slice thickness, and a 500-mm field-of-view (voxel resolution 0.97 mm). Filtered back projection reconstruction was used. Twenty-two patients were identified. The pre-RT CT, structure set, and dose maps, as well as the post-RT CT (from the second RT course) were downloaded onto a research workstation.

Landmark Pair Identification

A radiation oncologist (M.K.) utilized the previously validated semiautomated IX platform for identifying corresponding landmark pairs between pre-RT and post-RT images.[13] Initially, the software automatically generated candidate landmark points on the pre-RT image. Then, the user manually identified corresponding landmark pairs on the post-RT image utilizing the specialized software interface displaying both pre-RT and post-RT images in axial, sagittal, and coronal planes. The software aided in the visualization and selection of landmark pairs by using a thin-plate spline algorithm. However, since the software was only validated for temporal scans obtained during a single session (and not pre-RT vs post-RT scans), all landmark pairs were manually confirmed. Landmark pairs that could not be accurately identified for all pre-RT landmark points were labeled as undefined. The observer was not provided any other clinical or dosimetric information during the landmark identification process. One scan had such extensive fibrosis and retraction that landmarks could not be reliably identified for a large portion of the lung. That scan was eliminated, such that the final data set included 21 patients.

Pre-RT Lung Tumor and Post-RT Fibrosis Delineation

The pre-RT tumor volume was designated as the clinical gross tumor volume (GTV). Post-RT fibrotic regions were carefully delineated by a radiation oncologist (M.K.) using ITK-SNAP software, version 3.4.0.[14] Careful attention was placed toward including dense fibrotic regions.

Registration Algorithms

Post-RT scans were registered to pre-RT scans using 2 intensity-based B-spline deformable registration algorithms on the Elastix software platform, version 4.602.[12,15] All registrations were performed on an Intel Xeon E31225 3.10 GHz processor with 20 GB of RAM. Figure 1 is a schematic of the registration algorithms.

Control algorithm. Details of this algorithm have previously been published.[12] Briefly, an initial affine registration was followed by 2 nonrigid B-spline registrations using a multiresolution framework with the normalized correlation coefficient (NCC) metric. The first nonrigid registration was performed using the entire image. The second nonrigid registration incorporated a lung mask, which excluded regions outside of the lung parenchyma. The relative weight of the NCC metric to the bending energy term was 1 to 0.05. Five resolutions were utilized (first nonrigid registration [grid spacing/downsampling]: 80/16, 80/8, 40/4, 20/2, and 10/1 over 1000 iterations; second nonrigid registration: 40/5, 40/4, 20/3, 10/2, and 5/1 over 1000 iterations).

Line enhancement algorithm. This deformable registration algorithm was based on the same framework as the control algorithm. However, the pre-RT and post-RT images were
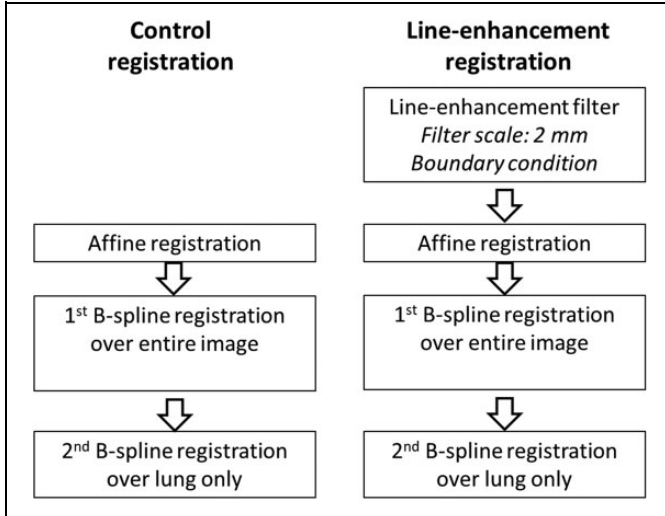
Figure 1. Schematic of control and line enhancement registration algorithms. The boundary condition for the line enhancement registration assigned all pixels outside of the lung parenchyma to the 99th percentile of the intensity values within the lung parenchyma of the line-enhanced image.

individually preprocessed with a line enhancement filter prior to the registration steps. This filter utilized a Hessian matrix for enhancing linear structures, such as the bronchial tree from the lung parenchyma. The Hessian matrix can be written as follows:

$$H = \begin{bmatrix} I_{xx} & I_{xy} & I_{xz} \\ I_{yx} & I_{yy} & I_{yz} \\ I_{zx} & I_{zy} & I_{zz} \end{bmatrix}, \quad (1)$$

where I_{xx} represents the partial second derivative of the image $I(x, y, z)$. This derivative was computed by convolving a Gaussian second derivative of scale σ, $G(x, y, z; \sigma)$, with $I(x, y, z)$, as shown in the following equation:

$$I_{xx} = \frac{\partial^2}{\partial x^2} G(x, y, z; \sigma) * I(x, y, z), \quad (2)$$

λ_1, λ_2, and λ_3 represent the eigenvalues of H, such that $\lambda_1 > \lambda_2 > \lambda_3$. The actual line filter was written as:

$$L = f(\lambda_1; \lambda_c) \times \lambda_c = \begin{cases} \lambda_c \exp\left(-\frac{\lambda_1^2}{2(\alpha_1 \lambda_c)^2}\right) & \lambda_1 \leq 0, \lambda_c \neq 0 \\ \lambda_c \exp\left(-\frac{\lambda_1^2}{2(\alpha_2 \lambda_c)^2}\right) & \lambda_1 > 0, \lambda_c \neq 0 \\ 0 & \lambda_c = 0 \end{cases}, \quad (3)$$

where $\lambda_c = \min(-\lambda_2, -\lambda_3) = -\lambda_2$.[11]

In this study, enhancement parameter values for α_1 and α_2 in Equation 3 were 0.5 and 2.0, respectively. These values were utilized in prior studies.[10,11] A filter scale σ of 2 mm was utilized in Equation 2 because it allowed for better suppression of the signal within the post-RT fibrotic region (Figure 2D) than the 3-mm scale line-enhanced image (Figure 2E), without introducing the numerous small linear intensities as in the 1-mm scale line-enhanced image (Figure 2C). Since the soft tissues of the chest wall (excluding the ribs) and the lung parenchyma exhibited similar intensity values in the line-enhanced images, a boundary condition, in which all pixels outside of the lung parenchyma were assigned to the 99th percentile of the intensity values within the lung parenchyma of the line enhancement image, was applied (see Figure 2F). Affine and B-spline deformable registrations of these line-enhanced images were then performed as in the control algorithm.

Registration Performance Assessment

The initial affine registration utilized for the control algorithm as well as the 2 deformable registration algorithms were evaluated using the following metrics:

1. Landmark error: The landmark error is the mean Euclidean distance measured in millimeters between the pre-RT landmark points and the transformed post-RT landmark points. This metric was computed for the entire lung, as well as for nonirradiated (equivalent dose in 2 Gy fractions [EQD2]; [α/β ratio = 3] 0-5 Gy) and irradiated (>5 Gy) lung. Undefined landmark points were not included in this analysis. Lower values of landmark error indicate better registration.
2. Overlap ratio: The overlap ratio (ie, Jaccard index) between the pre-RT and transformed post-RT lung masks was calculated. This metric represented the ratio of the intersection of the 2 masks over the union of the 2 masks, with 0 signifying no overlap, and 1 signifying complete overlap. Higher overlap ratios indicate a better registration.

Each metric was summarized by calculating the median value and the interquartile range (IQR) for all 21 cases. Wilcoxon signed rank tests were utilized to compare the line enhancement deformable registration with the control deformable registration with respect to landmark error and overlap ratio. Tests were statistically significant at a P value <.05.

Validation on External Data Set

The control and line enhancement deformable registration algorithms were also applied on an external data set of ten 4D-CT data sets with validated landmark pairs from the publicly available deformable image registration (DIR) reference database (http://www.dir-lab.com). The maximum inhalation and exhalation images were registered together. The landmark errors and overlap ratios were compared between the 2 algorithms using the Wilcoxon signed rank tests.
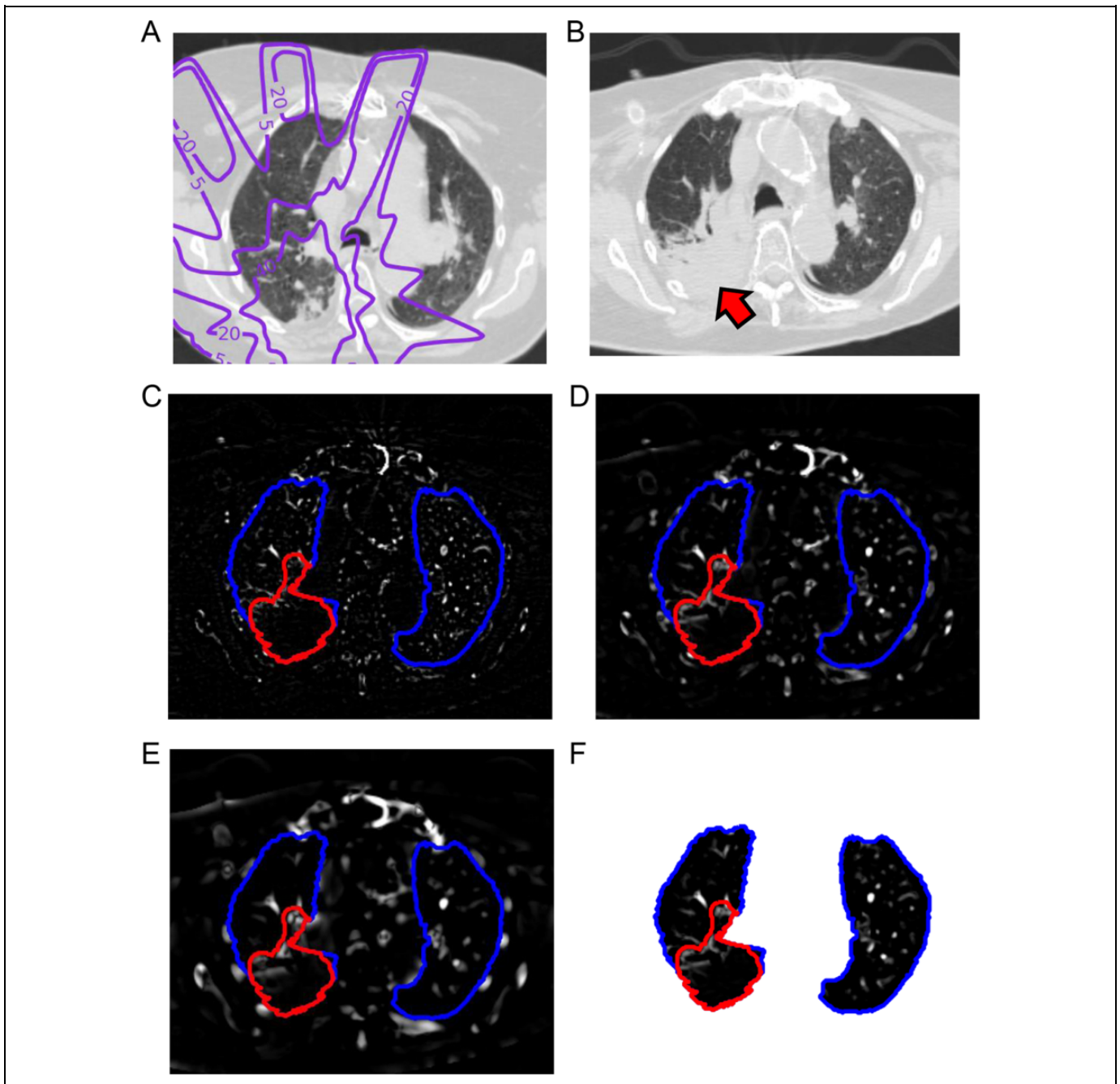
Figure 2. Images (L: -500; W: 1500) of a right upper lobe tumor treated with SBRT (50 Gy in 4 fractions). A, Pre-RT and (B) post-RT with fibrotic region (red arrow). C-E, Post-RT line enhancement images of (B) at scales of 1 mm (C), 2 mm (D), and 3 mm (E). F, Post-RT line enhancement image at 2-mm scale with boundary condition applied outside of lung parenchyma. Line enhancement images are scaled between minimum and maximum values within lung parenchyma. In (A), isodose lines (5, 20, and 40 Gy) are expressed in terms of equivalent dose in 2 Gy fractions (α/β ratio = 3). In (C-F), blue contours encircle lung parenchyma. Red contours encircle fibrotic region. RT indicates radiation therapy; SBRT, stereotactic body radiation therapy.

Impact of Factors on Registration Landmark Error for the Line Enhancement Registration

In order to elucidate the impact of specific factors on landmark error within the >5 Gy dose interval for line enhancement registration, Pearson correlation coefficients were calculated between the landmark error (>5 Gy interval) and the following factors: the presence of contrast on pre-RT and/or post-RT scans, the presence of pre-RT fiducial markers, treatment type (stereotactic body radiation therapy [SBRT] vs external beam radiation therapy [EBRT]), time between scans, pre-RT tumor size, post-RT fibrosis size, pre-RT tumor enhancement after line enhancement filtration (ratio of mean enhancement within tumor over maximum signal in lung parenchyma), post-RT

Table 1. Distribution of the Identified and Unidentified Landmark Pairs for the 0 to 5 Gy and >5 Gy Dose Intervals, Expressed in Equivalent Dose in 2 Gy Fractions (α/β Ratio = 3).

	Total Number of Pre-RT Landmarks		Number of Identified Landmark Pairs		Number of Unidentified Landmark Pairs		Percent of Identified Landmark Pairs (%)	
Dose (Gy)	Median	IQR	Median	IQR	Median	IQR	Median	IQR
0-5	74	51-84	71	50-81	1	0-3	98.7	95.4-100
>5	21	14-35	17	8-26	7	5-10	69.2	61.5-81.2
Total	100	97-100	90	76-92	8.0	6-13	91	86.0-93.0

Abbreviations: IQR, interquartile range; RT, radiation therapy.

Table 2. Performance Metrics for the Affine, Control Deformable, and Line Enhancement Deformable Registration Algorithms.[a]

	Affine Registration		Control Deformable Registration		Line Enhancement Deformable Registration		
Metrics	Median	IQR	Median	IQR	Median	IQR	P Value
Landmark error, mm	7.44	6.23-9.26	1.83	1.67-2.55	1.67	1.45-2.10	<.01
0-5 Gy	7.93	5.75-9.04	1.57	1.25-1.97	1.40	1.22-1.62	<.01
>5 Gy	10.31	8.43-11.15	3.31	2.30-4.57	2.25	1.80-3.92	<.01
Lung mask overlap ratio (%)	84.0	81.6-84.7	95.8	94.5-96.4	96.2	95.4-96.5	<.01

Abbreviation: IQR, interquartile range.
[a]All metrics were calculated over the entire lung, as well as nonirradiated (0-5 Gy) and irradiated (>5 Gy) regions. Dose is expressed in equivalent dose in 2 Gy fractions assuming an α/β ratio of 3. P values compare metrics between the 2 deformable registration algorithms.

fibrosis enhancement after line enhancement filtration, and the lung mask overlap ratio. Tests were statistically significant at a P value <.05. This analysis was also repeated for the difference in landmark errors within the >5 Gy dose interval between the line enhancement and control algorithms (see Supplemental Material S2). All statistical analysis was performed with the R statistical software v3.0 (The R Foundation for Statistical Computing, Vienna, Austria).

Results

Of the 21 patients included in this study, 15 cases had intravenous contrast enhancement on the pre-RT and/or post-RT scans, as determined by physician preference. Two patients had pre-RT fiducial markers. Fifteen patients received SBRT (EQD2 155 Gy; range: 104-276 Gy) and 6 patients received conventional EBRT (EQD2 74 Gy; range: 68-74 Gy). The median time interval between images was 1.2 years (range: 0.3-3.3 years). The median pre-RT tumor size was 11.4 cm³ (IQR: 7.1-39.0). The median intensity of the tumor after line enhancement filtration was 12.5% (IQR: 7.5-16.9). The median post-RT fibrosis size was 30.1 cm³ (IQR: 14.7-27.6), and the median intensity of the fibrosis after line enhancement filtration was 10.9% (IQR: 9.1-14.2). Twelve (57%) patients had a post-RT fibrotic volume that was more than double the size of the pre-RT tumor volume.

Landmark Pair Identification

As shown in Table 1, the median numbers of landmarks initially identified on the pre-RT image were 74 (IQR: 51-84) and 21 (14-35) for the 0 to 5 Gy and >5 Gy dose intervals, respectively. Landmark pairs were successfully identified for 98.7% (95.4-100) of the pre-RT landmarks for the 0 to 5 Gy dose interval but only 69.2% (61.5-81.2) for the >5 Gy dose interval. The median number of identified landmarks for the >5 Gy dose interval was 17 (IQR: 8-26).

Registration Performance Assessment

Table 2 shows performance metrics for the affine, control deformable, and line enhancement deformable (2-mm filter scale) registration algorithms. Median landmark errors (ie, median values of the 21 landmark errors, which were calculated as mean Euclidean distances between the pre-RT and transformed post-RT landmark points) for the affine algorithm were clearly inferior. Median landmark errors for the line enhancement algorithm were significantly lower than those for the control algorithm over the entire lung (1.67 vs 1.83; $P < .01$), as well as within the 0 to 5 Gy (1.40 vs 1.57; $P < .01$) and >5 Gy (2.25 vs 3.31; $P < .01$) dose intervals. Figure 3 shows box and whisker plots for the landmark errors on a per-case basis. The line enhancement algorithm exhibited lower landmark errors for 15 (71.4%) of the 21 cases in both 0 to 5 Gy and >5 Gy dose intervals.

We then conducted 2 additional comparisons. First, we performed our comparison of landmark errors for the subset of 15 cases with more than 8 landmark pairs (25th percentile) within the >5 Gy dose interval. There were statistically significant differences for the 0 to 5 Gy (median 1.57 [1.29-2.10] for control vs 1.34 [1.22-1.81] for line enhancement; $P = .05$) and >5 Gy (3.06 [2.30-4.15] vs 2.25 [1.84-2.96]; $P = .01$) dose
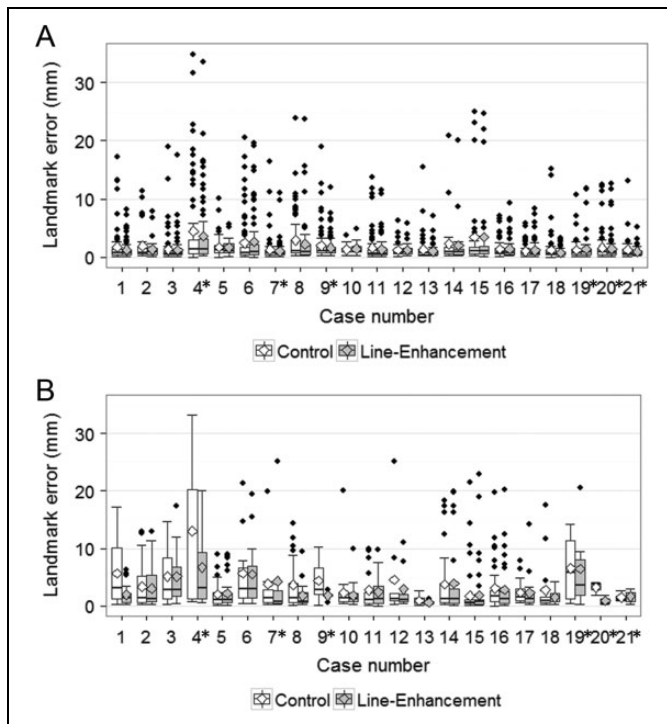
Figure 3. Box and whisker plots of landmark errors for the (A) 0 to 5 Gy and (B) >5 Gy dose intervals by the control and line enhancement deformable registration algorithms on a per-case basis. The dark lines within the boxes represent the median values, whereas the boxes span the IQR (25th-75th percentiles). The larger outlined diamonds represent mean values. The smaller shaded black diamonds above the whiskers represent outliers (greater than $1.5 \times$ IQR). *Refer to cases with 8 or less identified landmark pairs within the >5 Gy dose interval. IQR indicates interquartile range.

intervals. Second, we attempted to eliminate the effect of outlier points (shown in the box and whisker plots in Figure 3) by calculating landmark errors as the median Euclidean distance rather than mean Euclidean distance between pre-RT and transformed post-RT landmark points for each case. Among all 21 cases, there was no significant difference for the 0 to 5 Gy interval (median 0.90 [IQR: 0.72-1.13] for control vs 0.88 [0.74-1.06] for line enhancement; $P = .92$). However, there was a significant difference for the >5 Gy interval (1.73 [1.32-3.23] vs 1.36 [1.14-1.96]; $P = .01$).

The median lung mask overlap ratio for the line enhancement algorithm (96.2%) was greater than that for the control algorithm (95.8%; $P < .01$).

Validation on External Data Set

For the registrations from the external data set, there was no difference in landmark errors (median 1.33 [IQR: 1.17-1.52] for control vs 1.27 [1.15-1.44] for line enhancement; $P = .62$). There was also no difference in overall ratios (median 97.3 [96.4-97.7] for control vs 97.1 [96.5-97.4] for line enhancement; $P = .23$). Respective results for individual cases are shown in Supplemental Material S1.

Case Studies

Figure 2A-F had shown pre-RT, post-RT, and line-enhanced axial images of a right upper lobe (RUL) tumor treated with 50 Gy in 4 fractions of SBRT (case 9 in Figure 3). Figure 4 shows results from the deformable registrations of the post-RT image onto the pre-RT coordinate system. Notice that the large fibrotic region in the post-RT image (Figure 2B) was not well-preserved in the control registration (Figure 4A). The corresponding spatial Jacobian image (Figure 4C) showed marked variation, especially within the 2-cm expansion of the pre-RT GTV. Furthermore, the deformation fields (Figure 4E) depict marked warping in that vicinity, and the subtraction image (Figure 4G) shows marked warping of the postfibrotic region. On the other hand, the line enhancement registration (Figure 4B) showed much better preservation of the large fibrotic region, with far less variation in both the spatial Jacobian image (Figure 4D) and the deformation fields (Figure 4F). The fibrotic region is clearly delineated on the subtraction image (Figure 4H).

Figure 5A shows coronal images of a left upper lobe (LUL) tumor, treated with 40 Gy in 4 fractions of SBRT (case 20 in Figure 3). Figure 5B, acquired 1.4 years after RT, shows post-RT fibrosis around the LUL tumor, as well as the growth of a new RUL tumor outside of the high-dose RT field. Although both the control algorithm (Figure 5C) and the line enhancement registration (Figure 5E) displayed warping artifacts around the LUL tumor, the variation within the pre-RT GTV expansion of the spatial Jacobian image for the control registration (Figure 5D) was much greater than that for the line enhancement registration (Figure 5F). Furthermore, there was much more warping around the new RUL tumor for the control registration compared to that for the line enhancement registration.

Impact of Factors on Registration Landmark Error for the Line Enhancement Registration

Table 3 shows the results of the correlation analysis for landmark error within the >5 Gy dose interval. The only statistically significant factor was post-RT fibrosis enhancement ($P = .03$), which demonstrated an inverse relationship (correlation coefficient = −0.48) with landmark error as shown in Figure 6A. Figure 6B shows the series of images for 2 patients. Case 6 was a patient, who received SBRT (50 Gy in 4 fractions) to a left lower lobe tumor. The post-RT image was acquired 0.9 years later. The line enhancement filtration effectively suppressed both the pre-RT GTV and the post-RT fibrotic regions (post-RT fibrosis enhancement of 4.6%). Landmark errors within the >5 Gy dose interval for the line enhancement and control algorithms were 5.5 and 5.7 mm, respectively. Case 13 was a patient, who received SBRT (25 Gy in 1 fraction) to an RUL tumor. The post-RT image was acquired 0.8 years later. Although the line enhancement registration effectively suppressed much of the post-RT fibrotic volume, a prominent elongated structure remained (post-RT fibrosis enhancement
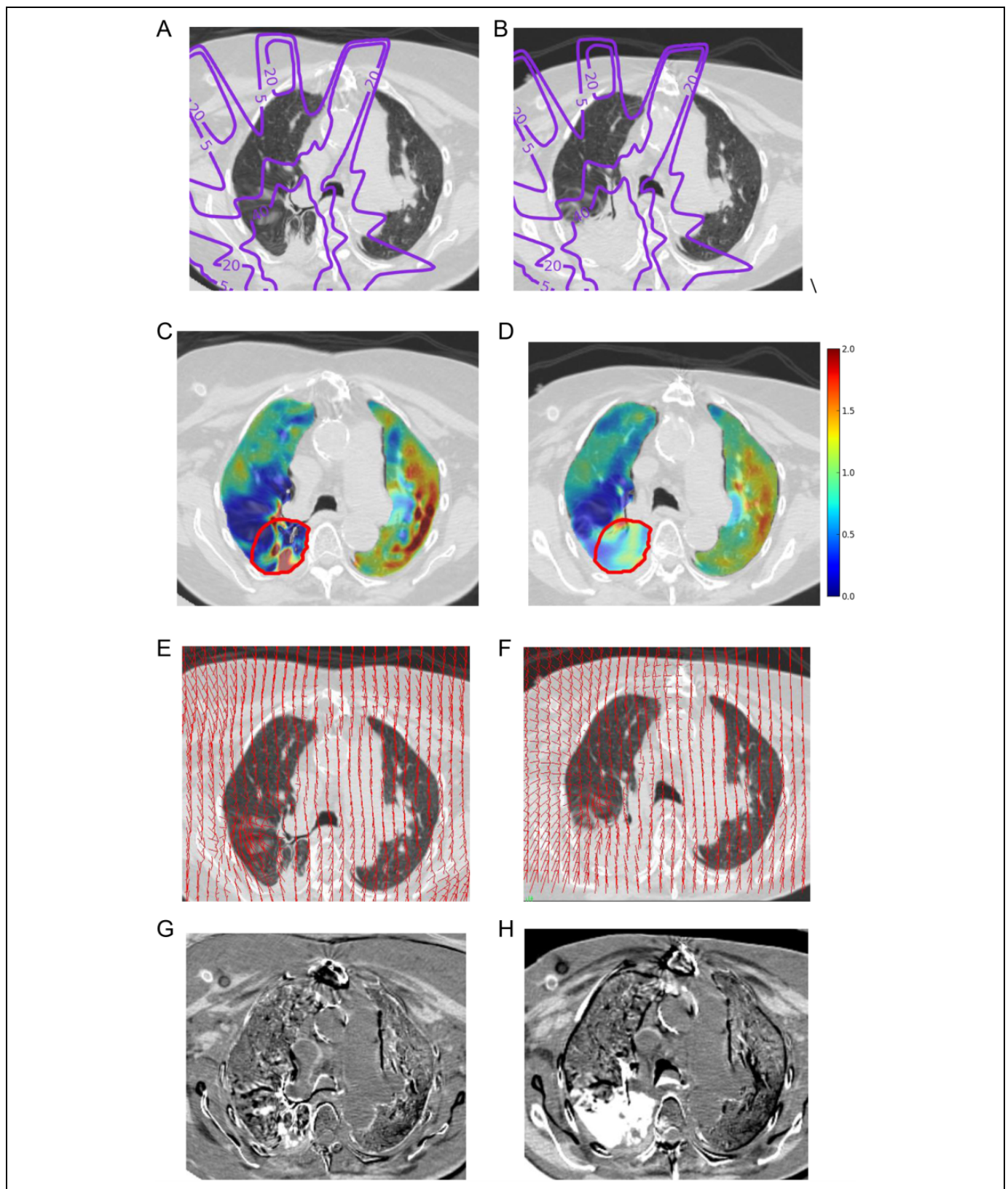
Figure 4. Registration images (L: -500; W: 1500) for the right upper lobe tumor treated with SBRT (50 Gy in 4 fractions) shown in Figure 2. A, Control registration image of the post-RT image, mapped onto the pre-RT coordinate system, with corresponding spatial Jacobian map, with values close to 1.0 signifying minimal deformation (C), deformable field (E), and subtraction image from pre-RT image (G). B, Line enhancement registration image of the post-RT image, mapped onto the pre-RT coordinate system, with corresponding spatial Jacobian map (D) deformation
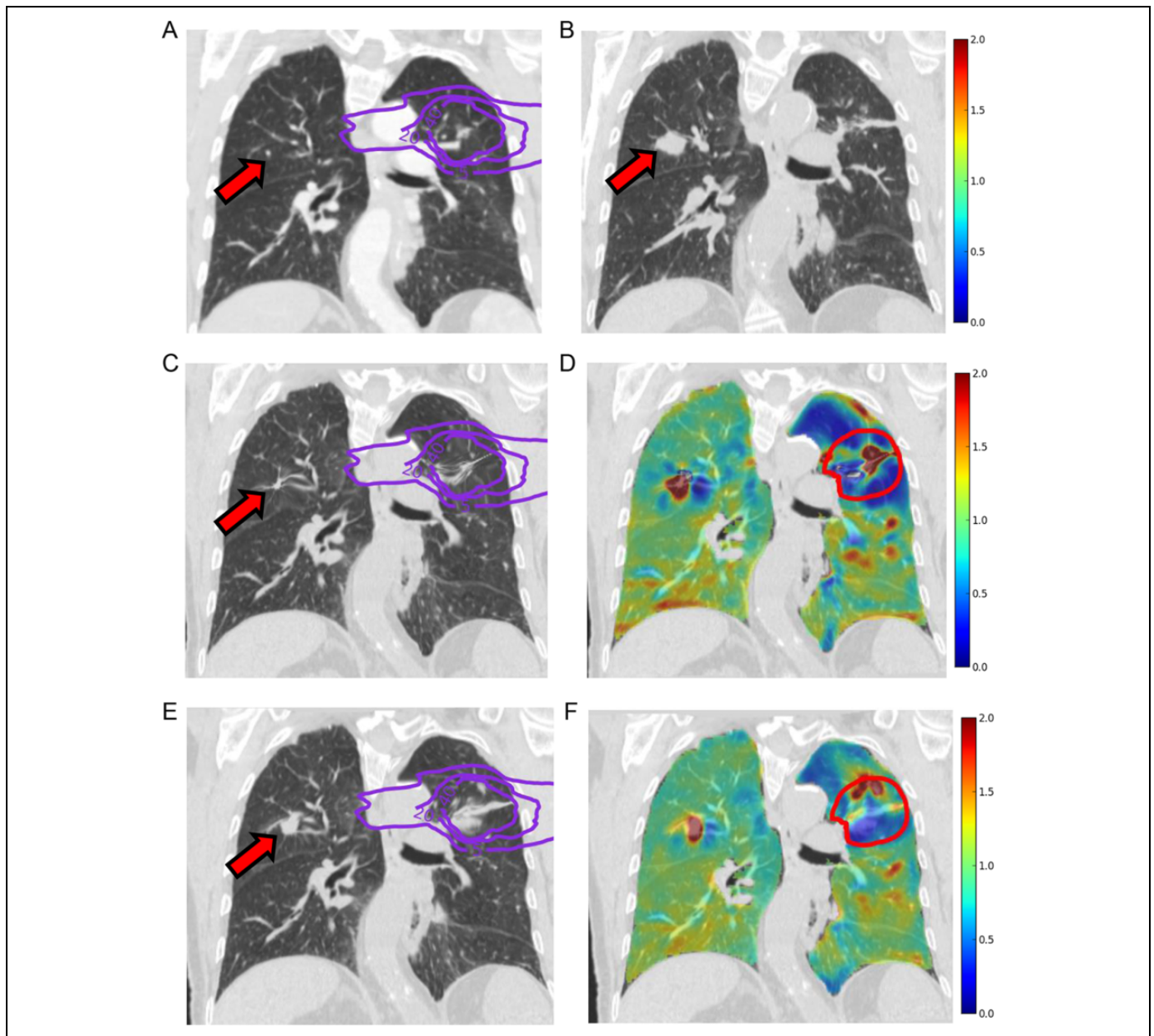
Figure 5. Images (L: -500; W: 1500) of a left upper lobe tumor (A) pre-RT and (B) post-RT acquired 1.4 years after stereotactic RT (40 Gy in 4 fractions). Red arrow points to growing right upper lobe tumor. C, Control registration image of the post-RT image, mapped onto the pre-RT coordinate system. D, Corresponding spatial Jacobian map, with values close to 1.0 signifying minimal deformation. E, Line enhancement registration image of the post-RT image, mapped onto the pre-RT coordinate system. F, Corresponding spatial Jacobian map. In (C) and (E), isodose lines (5, 20, and 40 Gy) are expressed in terms of equivalent dose in 2 Gy fractions (α/β ratio = 3). In (D) and (F), red circles represent the pre-RT GTV expanded by 2 cm within the lung parenchyma. GTV indicates gross tumor volume; RT, radiation therapy.

of 14.6%). A linear fibrotic structure of similar morphology was also present on the post-RT deformed image (post-RT image deformed onto the pre-RT coordinate system). When the deformed image was overlayed onto the pre-RT image, the linear fibrotic structure overlapped with a vessel bifurcation on the pre-RT image (green arrows in Figure 6B). Landmark errors within the >5 Gy dose interval for the line enhancement and control algorithms were 0.6 and 0.9 mm, respectively. These results suggest that the cases with maximally enhancing vasculature after suppression of fibrosis through line

Figure 4. (Continued). field (F), and subtraction image (H). The large white region in (H) corresponds to the preserved fibrotic region. In (A) and (B), isodose lines (5, 20, and 40 Gy) are expressed in terms of equivalent dose in 2 Gy fractions (α/β ratio = 3). In (C) and (D), red circles represent the pre-RT GTV expanded by 2 cm within the lung parenchyma. GTV indicates gross tumor volume; RT, radiation therapy; SBRT, stereotactic body radiation therapy.

Table 3. Pearson Correlation Coefficients of Landmark Error Within the 5 Gy Isodose Line Versus Individual Factors.

Factors	Coefficient	P
Pre-RT and/or post-RT contrast	0.33	.15
Pre-RT fiducial markers	−0.20	.39
SBRT vs EBRT	0.17	.74
Time between scans	−0.35	.12
Pre-RT tumor size	−0.02	.95
Post-RT fibrosis size	0.27	.23
Pre-RT tumor enhancement	−0.11	.63
Post-RT fibrosis enhancement	−0.48	.03[a]
Lung mask overlap ratio	−0.15	.50

Abbreviations: EBRT, external beam radiation therapy; RT, radiation therapy; SBRT, stereotactic body radiation therapy.
[a]Signifies statistical significance at a P value <.05.

enhancement filtration had lower landmark errors within the >5 Gy dose interval than those with minimal enhancement. Enhancing vasculature after line enhancement filtration may play an important role in ensuring accuracy after DIR.

As shown in Supplemental Material S2, pre-RT tumor enhancement was the only factor to demonstrate a significant association with the landmark error difference (line enhancement minus control) within the >5 Gy dose interval ($r = -0.53$; $P = .01$). These results suggest that the line enhancement registration algorithm was not able to improve landmark error for cases in which there remained minimal enhancing signal after line enhancement filtration. In other words, residual signal within the tumor volume appeared to positively influence registration results for this algorithm as compared to the control algorithm.

Discussion

In this article, we demonstrated the feasibility of incorporating a line enhancement filter into a deformable registration algorithm for aligning pre-RT and post-RT images. Since the median time interval between the pre-RT and post-RT scans was 1.2 years, the post-RT images were affected by radiation fibrosis, with 12 of 21 patients having a post-RT fibrosis volume that was more than double that of the pre-RT tumor volume. The line enhancement registration algorithm significantly decreased landmark error in the entire lung, as well as the nonirradiated and irradiated regions when compared to the control algorithm. Furthermore, this algorithm preserved the overlap ratio in the entire lung.

The line enhancement filter improved the deformable registration result because it effectively suppressed the homogeneous intensities present within the pre-RT GTV and the post-RT fibrotic regions. By suppressing these regions, the line enhancement filter allowed for the deformable registration to focus primarily on matching the line-enhanced vascular structures, which were more likely to be concordant between the pre-RT and post-RT images. The pre-RT and post-RT homogeneous regions, on the other hand, were more likely to be discordant due to the effect of RT. The control registrations often exhibited prominent distortions around the tumor because the algorithm attempted to match the often larger post-RT fibrotic regions to the smaller pre-RT tumors (see Figure 4A).

An interesting result was the statistically significant inverse relationship between post-RT fibrosis enhancement after line enhancement filtration and landmark error (correlation coefficient = −0.48; $P = .03$). No other evaluated factor, including treatment type (SBRT vs EBRT), post-RT fibrosis size, or time between scans, demonstrated a statistically significant relationship. As shown in case 13 in Figure 6B, some of the post-RT fibrosis enhancement may have included pulmonary vessels, which became enveloped by radiation-induced fibrosis. These results suggest that the line enhancement algorithm improved landmark error within irradiated regions by suppressing homogeneous fibrotic regions while enhancing underlying vessels. The deformable registration algorithm could then register these enhanced vascular structures in the post-RT image to the enhanced vascular structures in the pre-RT images.

Previous investigators have utilized line enhancement filters for improving the deformable registration of pulmonary CT images. Cao *et al* demonstrated that adding a line enhancement similarity cost function to an intensity-based deformable registration algorithm allowed for a 25% decrease in landmark positioning error among CT images corresponding to different respiratory phases in 6 patients,[16] with a mean registration error of 0.74 mm (standard deviation [SD]: 0.57 mm) when the NCC was used. Hugo *et al* applied such an algorithm for registering images that demonstrated tumor regression during RT in a 3 patient series.[17] The mean registration error in that study was 3.3 mm (SD: 2.4 mm). Most recently, Cazoulat *et al* incorporated line enhancement registration into a biomechanical deformable model for registering treatment planning images with post-RT images acquired 3 weeks after external beam therapy in a series of 6 patients.[10] The mean registration error in that study was 1.6 mm (SD: 1.3 mm). This study, on the other hand, focused on the registration of pre-RT and post-RT images acquired months after therapy completion in a much larger cohort. The mean value of all 21 landmark errors for the line enhancement algorithm was 1.87 mm (SD: 0.74). The presence of radiation fibrosis in most of the patients allowed us to highlight the utility of the line enhancement algorithm for the DIR of pre-RT and post-RT images.

A key strength of this study was the inclusion of 21 cases, treated with contemporary EBRT and SBRT techniques through a wide follow-up range from 0.3 to 3.3 years. Our finding that the line enhancement algorithm performed better than the control algorithm with respect to landmark error, and overlap ratio, gives us confidence that this algorithm would be applicable to the wide variety of pneumonitis/fibrosis patterns encountered after RT.[18,19] A limitation of the study was the difficulty in identifying landmark pairs in irradiated regions, as manifested by the 69.2% rate of identifying landmark pairs within the >5 Gy dose interval. Landmark errors were often difficult to identify, due to ground glass opacities, dense consolidative changes, and traction bronchiectasis causing
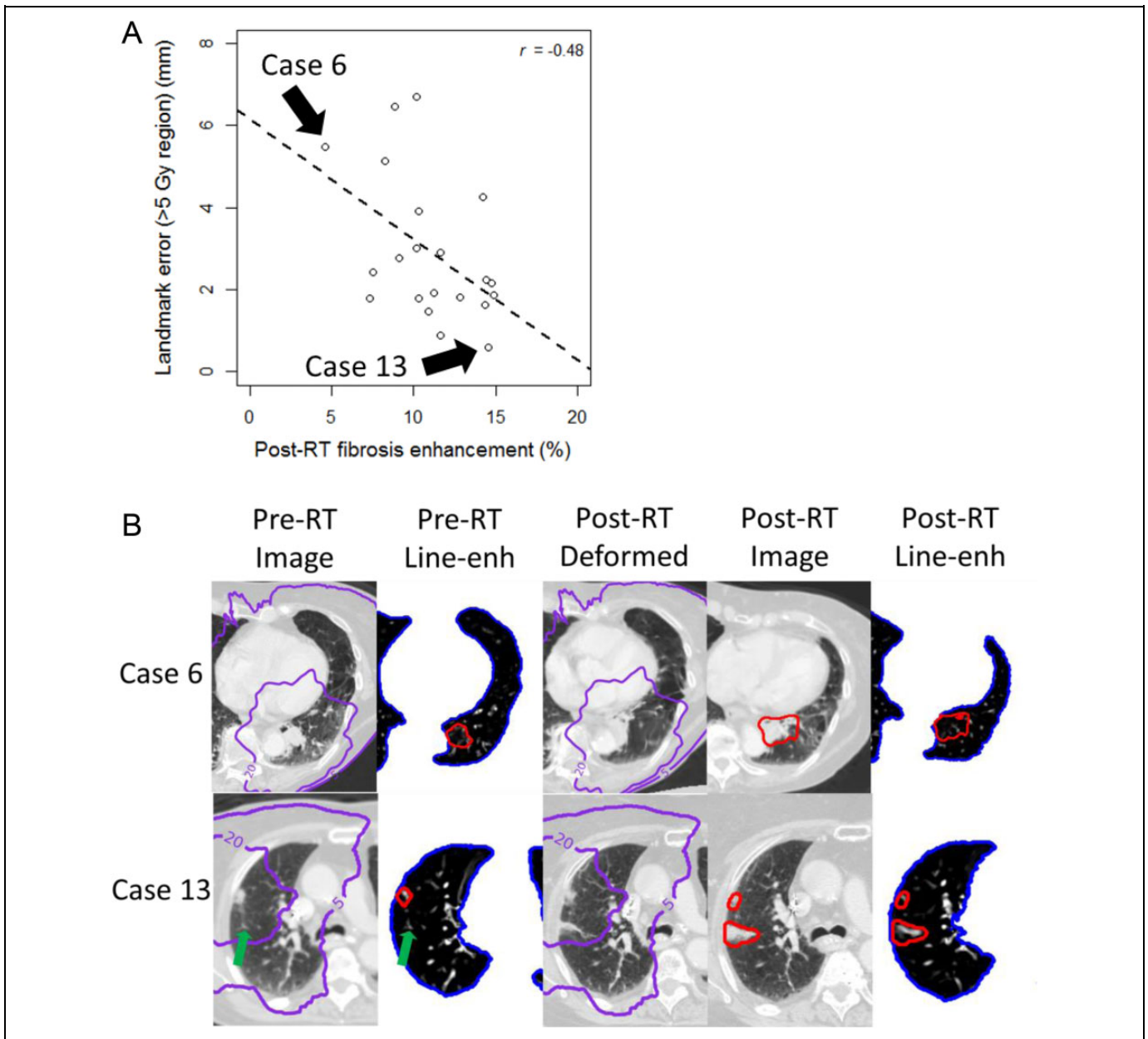
Figure 6. A, Plot of landmark error within >5 Gy region versus post-RT fibrosis enhancement for line enhancement registration. Case numbers correspond to those shown in Figure 3. B, Panel of pre-RT and post-RT images. Isodose lines (5 and 20 Gy) are expressed in terms of equivalent dose in 2 Gy fractions (α/β ratio = 3). Red circles represent the pre-RT GTV and post-RT fibrosis for pre-RT and post-RT images, respectively. Note the lack of enhancement within the contoured post-RT line-enhanced image for case 6, and the presence of enhancement for case 13. In case 13, green arrows point to a vessel bifurcation on the pre-RT images that corresponds to the elongated structure within the post-RT line-enhanced image. GTV indicates gross tumor volume; RT, radiation therapy.

complex deformation of surrounding parenchyma.[19] However, in the subset of 15 patients who had more than 8 landmark pairs within the >5 Gy dose interval, the line enhancement algorithm exhibited a lower landmark error than the control algorithm.

An additional limitation is that the line enhancement registration results were not ideal for all of the cases presented in this study. As shown in Figure 6A, 5 of the 21 cases had a registration error within the irradiated region (>5 Gy) greater than 4 mm. Landmark errors for the control algorithm were even greater for 4 of these 5 cases. For both algorithms, cases with large landmark errors often had post-RT fibrotic regions that retracted large portions of the adjacent parenchyma. Rational methods that could compensate for these large retractions prior to deformable registration may be needed.[20] Other potential modifications include optimizing the line enhancement filter settings, incorporating multiple scales into the filter,[21] adjusting the boundary condition for pixels outside of the lung parenchyma, or considering other

deformable registration algorithms.[22] Future studies in improving the line enhancement registration algorithm as well as validating the results of this study in multi-institutional data sets are needed.

Acknowledgments

Declaration of Conflicting Interests

Funding

Supplemental Material

Supplementary material for this article is available online.

References

1. Liu H, Zhang X, Vinogradskiy YY, Swisher SG, Komaki R, Chang JY. Predicting radiation pneumonitis after stereotactic ablative radiation therapy in patients previously treated with conventional thoracic radiation therapy. *Int J Radiat Oncol Phys*. 2012;84(4):1017-1023. doi:10.1016/j.ijrobp.2012.02.020.

2. Ruysscher DD, Faivre-Finn C, Pechoux CL, Peeters S, Belderbos J. High-dose re-irradiation following radical radiotherapy for non-small-cell lung cancer. *Lancet Oncol*. 2014;15(13):e620-e624. doi:10.1016/S1470-2045(14)70345-6.

3. Binkley MS, Hiniker SM, Chaudhuri A, et al. Dosimetric factors and toxicity in highly conformal thoracic reirradiation. *Int J Radiat Oncol Biol Phys*. 2016;94(4):808-815. doi:10.1016/j.ijrobp.2015.12.007.

4. Ding K, Bayouth JE, Buatti JM, Christensen GE, Reinhardt JM. 4DCT-based measurement of changes in pulmonary function following a course of radiation therapy. *Med Phys*. 2010;37(3):1261. doi:10.1118/1.3312210.

5. Vinogradskiy Y, Diot Q, Kavanagh B, Schefter T, Gaspar L, Miften M. Spatial and dose–response analysis of fibrotic lung changes after stereotactic body radiation therapy. *Med Phys*. 2013;40(8):081712. doi:10.1118/1.4813916.

6. King MT, Maxim PG, Diehn M, Loo BW, Xing L. Analysis of long-term 4-dimensional computed tomography regional ventilation after radiation therapy. *Int J Radiat Oncol Biol Phys*. 2015; 92(3):683-690. doi:10.1016/j.ijrobp.2015.02.037.

7. Cunliffe AR, White B, Justusson J, et al. Comparison of two deformable registration algorithms in the presence of radiologic change between serial lung CT scans. *J Digit Imaging*. 2015; 28(6):755-760. doi:10.1007/s10278-015-9789-1.

8. Staring M, Klein S, Pluim JPW. A rigidity penalty term for non-rigid registration. *Med Phys*. 2007;34(11):4098-4108. doi:10.1118/1.2776236.

9. Sakamoto R, Mori S, Miller MI, Okada T, Togashi K. Detection of time-varying structures by large deformation diffeomorphic metric mapping to aid reading of high-resolution CT images of the lung. *PLoS One*. 2014;9(1):e85580. doi:10.1371/journal.pone.0085580.

10. Cazoulat G, Owen D, Matuszak MM, Balter JM, Brock KK. Biomechanical deformable image registration of longitudinal lung CT images using vessel information. *Phys Med Biol*. 2016; 61(13):4826-4839. doi:10.1088/0031-9155/61/13/4826.

11. Sato Y, Nakajima S, Atsumi H, et al. 3D multi-scale line filter for segmentation and visualization of curvilinear structures in medical images. In: *CVRMed-MRCAS'97*. Springer; 1997:213-222. http://link.springer.com/chapter/10.1007/BFb0029240. Accessed November 28, 2016.

12. Staring M, Klein S, Reiber JH, Niessen WJ, Stoel BC. Pulmonary image registration with elastix using a standard intensity-based algorithm. *Med Image Anal Clin Gd Chall*. 2010;2010:73-79.

13. Murphy K, van Ginneken B, Klein S, et al. Semi-automatic construction of reference standards for evaluation of image registration. *Med Image Anal*. 2011;15(1):71-84. doi:10.1016/j.media.2010.07.005.

14. Yushkevich PA, Piven J, Hazlett HC, et al. User-guided 3D active contour segmentation of anatomical structures: significantly improved efficiency and reliability. *Neuroimage*. 2006;31(3):1116-1128.

15. Klein S, Staring M, Murphy K, Viergever M, Pluim JPW. Elastix: a toolbox for intensity-based medical image registration. *IEEE Trans Med Imaging*. 2010;29(1):196-205. doi:10.1109/TMI.2009.2035616.

16. Castillo E, Castillo R, Martinez J, Shenoy M, Guerrero T. Four-dimensional deformable image registration using trajectory modeling. *Phys Med Biol*. 2010;55(1):305. doi:10.1088/0031-9155/55/1/018.

17. Cao K, Ding K, Reinhardt JM, et al. Improving intensity-based lung CT registration accuracy utilizing vascular information. *Int J Biomed Imaging*. 2012;2012:285136. doi:10.1155/2012/285136, 10.1155/2012/285136.

18. Hugo GD, Cao K, Guy C, Weiss E, Jan N, Christensen GE. Measurement of local deformation due to lung tumor response to radiation therapy. In: Beichel RR, de Bruijne M, Kabus S, et al., eds. *The Fifth International Workshop on Pulmonary Image Analysis*. Nagoya, Japan; 2013:97-108. http://www.lungworkshop.org/2013/resources/2013_Proc_IWPIA5_HugoEtAl.pdf. Accessed April 27, 2016.

19. Libshitz HI, Shuman LS. Radiation-induced pulmonary change: CT findings. *J Comput Assist Tomogr*. 1984;8(1):15-19.

20. Takeda T, Takeda A, Kunieda E, et al. Radiation injury after hypofractionated stereotactic radiotherapy for peripheral small lung tumors: serial changes on CT. *Am J Roentgenol*. 2004; 182(5):1123-1128. doi:10.2214/ajr.182.5.1821123.

21. Schreibmann E, Xing L. Image registration with auto-mapped control volumes. *Med Phys*. 2006;33(4):1165-1179. doi:10.1118/1.2184440.

22. Sato Y, Nakajima S, Shiraga N, et al. Three-dimensional multi-scale line filter for segmentation and visualization of curvilinear structures in medical images. *Med Image Anal*. 1998;2(2):143-168. doi:10.1016/S1361-8415(98)80009-1.